Structural Chemistry (2019) 30:2167–2180
https://doi.org/10.1007/s11224-019-01331-y

ORIGINAL RESEARCH

Exploring the transfer of hydrogen atom from kaempferol-based compounds to hydroxyl radical at ground state using PCM-DFT approach

Khajadpai Thipyapong[1] · Nuttawisit Yasarawan[1]

Received: 24 February 2019 / Accepted: 29 March 2019 / Published online: 3 May 2019

Abstract

Thermodynamic and kinetic studies of the hydrogen atom transfer (HAT) from hydroxyl (OH) groups of four kaempferol-based compounds, namely kaempferol, morin, morin-5*-sulfonate and morin-7-O-sulfate to hydroxyl radical (·OH), have been carried out using density functional theory (DFT) methods at the CAM-B3LYP/6–311++G(d,p) level equipped with polarizable continuum model (PCM) of solvation. All HAT reactions in aqueous solution are exothermic and spontaneous. For most compounds, the most preferable OH group for HAT is situated at position C3 (O3-H3) on the pyrone ring. The reaction potential of such a reactive group is found to be highest in morin-7-O-sulfate. The rate constants for the HAT reactions at different OH groups of each compound have been determined based on the transition state theory. The presence of substituents leads to the variation in either the characteristic interactions at the reactive site or the charge distribution on transition-state geometries, hence significantly affecting the kinetics of HAT. The highest rate of HAT is resulted for the OH group at position C4* (O4*-H4*) on the phenyl ring (ring B) of morin-5*-sulfonate because a hydrogen bond between ·OH and the sulfonate group favors the formation of transition state. However, for most compounds under study, the HAT reaction at O3-H3 initiated by ·OH is highly favorable both thermodynamically and kinetically.

Keywords Flavonoids · Hydroxyl radical · Hydrogen atom transfer · DFT · PCM

Introduction

3-Hydroxyflavone and its hydroxylated derivatives form a class of phytophenolic compounds known as flavonols belonging to the flavonoid family. The diversity of flavonols in nature basically stems from the variation in the number and/or position of their hydroxyl (OH) groups. Among all natural flavonols known to date, kaempferol and morin have received considerable attention due to their diverse medicinal benefits [1–4]. In terms of molecular structure, as shown in Scheme 1, both kaempferol and morin bear the same chromone moiety which is a benzene ring (ring A) fused with a 4-pyrone ring (ring C). Ring C has a phenyl ring (ring B) substituted at position C2. As seen in Scheme 1, morin is in fact a C2*-hydroxylated derivative of kaempferol. The antioxidant activity, which is perhaps the best known therapeutic property of flavonols, emerges from their capability to scavenge the unbalanced amounts of reactive oxygen and nitrogen radical species that cause oxidative damages to various biomolecules such as proteins, lipids, and DNA [5, 6]. As the activities of pharmaceutical agents are usually dependent on both the molecular structure and the pattern of substituents, a great deal of work has been carried out to establish the relationship between the structures and the radical-scavenging activity of flavonols [7].

Hydroxyl radical (·OH) is one of the most reactive oxyradicals found commonly in biological systems and atmosphere [7]. The pioneering experiment based on the spin-trapping technique has demonstrated that the scavenging activity of natural flavonols toward ·OH increases with the number of OH groups substituted on ring B [8]. The previous structure-activity relationship (SAR) analysis of various natural flavonoids has indicated that only the OH-containing flavonoids are active in scavenging, ·OH and the radical-

Electronic supplementary material The online version of this article (https://doi.org/10.1007/s11224-019-01331-y) contains supplementary material, which is available to authorized users.

✉ Nuttawisit Yasarawan
nuttawisit@buu.ac.th

[1] Department of Chemistry, Faculty of Science, Burapha University, Chonburi 20131, Thailand

Scheme 1 Sketches of four kaempferol-based molecules with the atom numbering.

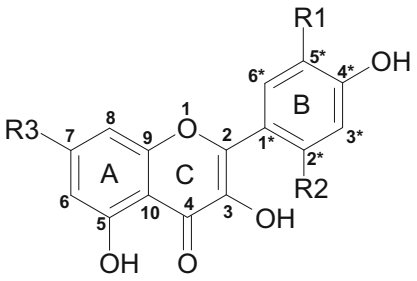

Compound	R1	R2	R3
Kaempferol	–H	–H	–OH
Morin	–H	–OH	–OH
Morin-5*-sulfonate	$–SO_3^-$	–OH	–OH
Morin-7-O-sulfate	–H	–OH	$–OSO_3^-$

scavenging activity of OH groups on ring B is higher than that of OH groups on ring A [9]. It has been widely accepted that the potency of kaempferol and other flavonols to scavenge ·OH relies on their ability to donate hydrogen atoms to ·OH. Basically, the attack of ·OH at a reactive OH group in a given kaempferol-based molecule initiates the following hydrogen atom transfer (HAT) reaction:

$$R{-}OH + OH \rightarrow R{-}O + H_2O. \quad (1)$$

where R-OH and R-O· represent the kaempferol-based compound (hydroxylated compound) and its respective oxyradical product, respectively. The previous work has reported that flavonoids thermodynamically prefer the HAT mechanism in polar media [10]. Nevertheless, most flavonols including kaempferol and morin are slightly soluble in water at the physiological pH value; this could considerably limit their pharmaceutical applications [4, 11]. Such a drawback can be overcome by chemically replacing OH group with an anionic substituent. Recently, the preparation of water-soluble morin derivatives such as morin-5*-sulfonate and morin-7-O-sulfate (see Scheme 1) has been reported [3, 4, 12]. It has been suggested in the previous work that morin-7-O-sulfate could be an anticancer due to its role as a signal transduction inhibitor in targeted therapies of melanoma [12]. To our best knowledge, there has been no information in the literature regarding the HAT reactions of morin-5*-sulfonate and morin-7-O-sulfate until the present day. Apart from various experimental techniques, density functional theory (DFT) methods have been widely used in characterizing the hydrogen transfer phenomena in several organic molecules including flavonoids in either ground or excited states [13–16]. DFT calculations have been proven useful in predicting the reactivity of several flavonoids [17, 18]. In the present study, the stable geometries in water of the kaempferol-based compounds shown in Scheme 1: kaempferol, morin, morin-5*-sulfonate, and morin-7-O-sulfate have been determined by means of full geometry optimization with DFT methods under polarizable continuum model (PCM) of solvation. Thermodynamic and kinetic parameters for the ground-state hydrogen atom abstraction from different OH groups in all studied kaempferol-based compounds by the radical ·OH in aqueous solution have been theoretically evaluated. While a number of previous works have focused on either finding the relationship between the O–H bond dissociation enthalpies of flavonols and their radical-scavenging activities or addressing the most preferable OH groups for radical attack, the present work has aimed at gaining fundamental insights into the structural effect on the activation process of the HAT reaction at each reactive site of molecule. The mechanistic details of HAT based on the transition state theory have been addressed. A variety of interactions such as hydrogen bonding and electrostatic forces that affect the stability of the transition-state geometries and the dependence of these interactions on the choice of substituent have been analyzed. Allowing for the polyhydroxy nature of all kaempferol-based compounds in the present study, there are already 18 HAT reactions to be considered. Thus, it is necessary to declare that either the attack of ·OH at the regions other than the OH groups of compounds or other reaction mechanisms besides HAT or further reactions of the oxyradical products are beyond the scope of this work.

Computational details

Ground-state geometries of all compounds under study were fully optimized with the *Gaussian 16* program package [19] using DFT methods. The long-range-corrected functional CAM-B3LYP (i.e., B3LYP combined with coulomb-attenuating method to account for the long-range HF exchange interactions) [20] was used in all cases. Previously, CAM-B3LYP has been reported as being more effective in predicting electronic properties than the conventional B3LYP [16, 21]. The Pople split-valence triple-zeta basis set such as 6–311++G(d,p) was adopted to all computations. For such a basis set, the core orbital is described by a contracted set of six primitive Gaussian functions, and the valence orbital by a contracted set of three primitive Gaussian functions and two other sets of one Gaussian function. The notation ++ indicates that a set of diffuse functions are included to heavy

atoms and hydrogen. As HAT is the main theme of this work, including diffuse functions to all hydrogen atoms is necessary. The notation (d,p) indicates the inclusion of d-polarization functions to non-hydrogen atoms and p-polarization functions to hydrogen atoms. The 6–311++G(d,p) basis set has been used to describe the hydrogen transfer phenomena in various organic compounds [16, 22–24]. Importantly, DFT calculations at the CAM-B3LYP/6–311++G(d,p) level can accurately predict both the structural and spectroscopic data of 3-hydroxyflavone and morin [25]. The optimized ground-state geometries of compounds were taken to the process of vibrational frequency calculations, in which the zero-point corrected electronic energies, partition functions, and thermodynamic parameters were evaluated. Solvation effect was taken into account by the application of polarizable continuum model (PCM). In this solvation methodology, the solute molecule was placed in a theoretical cavity surrounded by a polarizable dielectric continuum of water (dielectric constant = 78.39). The non-electrostatic component of the free energy of solvation and atomic radii for such a solvation cavity were defined based on the solute electron density [26]. Natural population analysis was performed using the *NBO Version 3.1* program [27] integrated within the *Gaussian 16* program suite to obtain useful sets of natural bond orbital (NBO) data, e.g., atomic charges, electron populations, and donor-acceptor orbital interaction energies. Electrostatic force between atom A and atom B (F_{AB}) can be estimated using Coulomb's relation:

$$F_{AB} = \frac{q_A q_B}{r^2} \tag{2}$$

where $q_A q_B$ and r are the product of charges on both atoms and the interatomic distance, respectively. The optimized transition-state (TS) geometries were obtained using either the synchronous transit-guided quasi-Newton (STQN) method or the Berny optimization method. The presence of a single imaginary vibrational frequency that is consistent with the progress of HAT was used as an indication of the optimized geometry being a transition state. The proper connectivity between reactants, transition states, and products were validated for all reaction pathways using intrinsic reaction coordinate (IRC) calculations. The rate constant (k) for the attack of ·OH on the kaempferol-based compound at the temperature T can be determined using the relation [28]:

$$k = \kappa \frac{k_B T}{h} \frac{Q^{TS}}{Q^{PR}} exp\left(-\Delta E^{\ddagger}/RT\right) \tag{3}$$

where k_B, h, and R are the Boltzmann constant, the Planck constant, and the universal gas constant, respectively. Q^{TS} and Q^{PR} denote the total partition functions of the transition-state (TS) geometry and the pre-reactive complex (i.e., the kaempferol-based molecule with ·OH hydrogen-bonded to its reactive OH group), respectively. The activation energy of reaction, $\Delta E^{\ddagger}$, was determined as the energy difference between the TS geometry and the pre-reactive complex. The Wigner transmission coefficient, κ, which accounts for the barrier-tunneling correction, is calculated as [29]

$$\kappa = 1 + \frac{1}{24}\left(\frac{h\nu_i}{k_B T}\right)^2, \tag{4}$$

where ν_i is the imaginary part of the vibrational frequency of the transition-state geometry.

Results and discussion

Conformational analysis of kaempferol-based compounds

According to the potential plots shown in Fig. 1, there exist two stable rotamers, both of which can be interconverted by rotating ring B (planar ring) about C2-C1* (single bond). In the case of kaempferol, as ring B is symmetric to such a rotation, this parent compound simply has only one stable conformation (no rotamer). Ring B in the most stable conformation of kaempferol, with the torsion angle O1-C2-C1*-C2* of about 180°, is obviously coplanar with the other two rings. The less stable rotamers of morin and its two derivatives show the values of torsion angle O1-C2-C1*-C2* lower than 5°, suggesting that the O2*-H2* group on ring B is located on the same side as O1 (pyranyl O atom on ring C), and ring B is almost coplanar with ring C. The optimized geometries of the more stable rotamers are displayed in Fig. 2 with their electrostatic potential surfaces. These rotamers show the values of torsion angle O1-C2-C1*-C2* in the range of 150°–160°. This result indicates that the O2*-H2* group in each of the more stable rotamers is located on the same side as O3 (the hydroxyl O atom), but ring B is not perfectly coplanar with ring C. These structural characteristics of the more stable rotamers predicted in this work agree well with the crystallographic data of morin-5*-sulfonate in its chelate forms [4]. The vibrational frequency at 1200 cm^{-1} for the asymmetric S-O stretching in the more stable rotamer of morin-5*-sulfonate in gas phase computed at the CAM-B3LYP/6–311++G(d,p) level is satisfactorily close to the experimental value at 1197 cm^{-1} [4]. As the presence of intramolecular hydrogen bond is the cause of high conformational stability, O3···H2* in each of the more stable rotamer is expected to be stronger than O1···H2* in the respective less stable rotamer. The O3-H2* attractive force (e^2 $Å^{-2}$) in the more stable rotamer is found to increase in the order: morin-5*-sulfonate (− 0.1318) < morin (− 0.1323) < morin-7-O-sulfate (− 0.1375). The O1-H2* attractive force (e^2 $Å^{-2}$) in the less stable rotamer increases in the order: morin-5*-sulfonate (-8.50×10^{-2}) < morin (-8.56×10^{-2}) < morin-7-O-sulfate ($-9.02 \times$

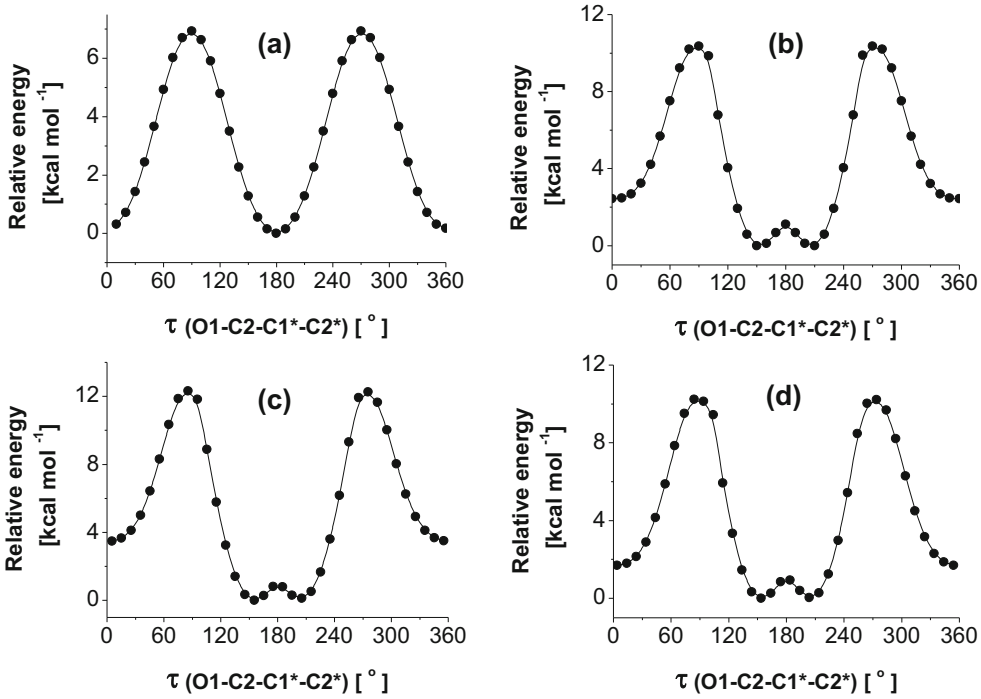

Fig. 1 Potential energy scans as a function of the torsion angle O1-C2-C1*-C2*. **a** Kaempferol. **b** Morin. **c** Morin-5*-sulfonate. **d** Morin-7-O-sulfate

10^{-2}). Based on the magnitudes of electrostatic forces between O and H atoms, O3···H2* in the more stable rotamer is essentially stronger than O1···H2* in the less stable rotamer. Furthermore, the strongest hydrogen bonding is resulted in morin-7-O-sulfate. Henceforth, the further theoretical investigation will be dedicated to the more stable rotamers.

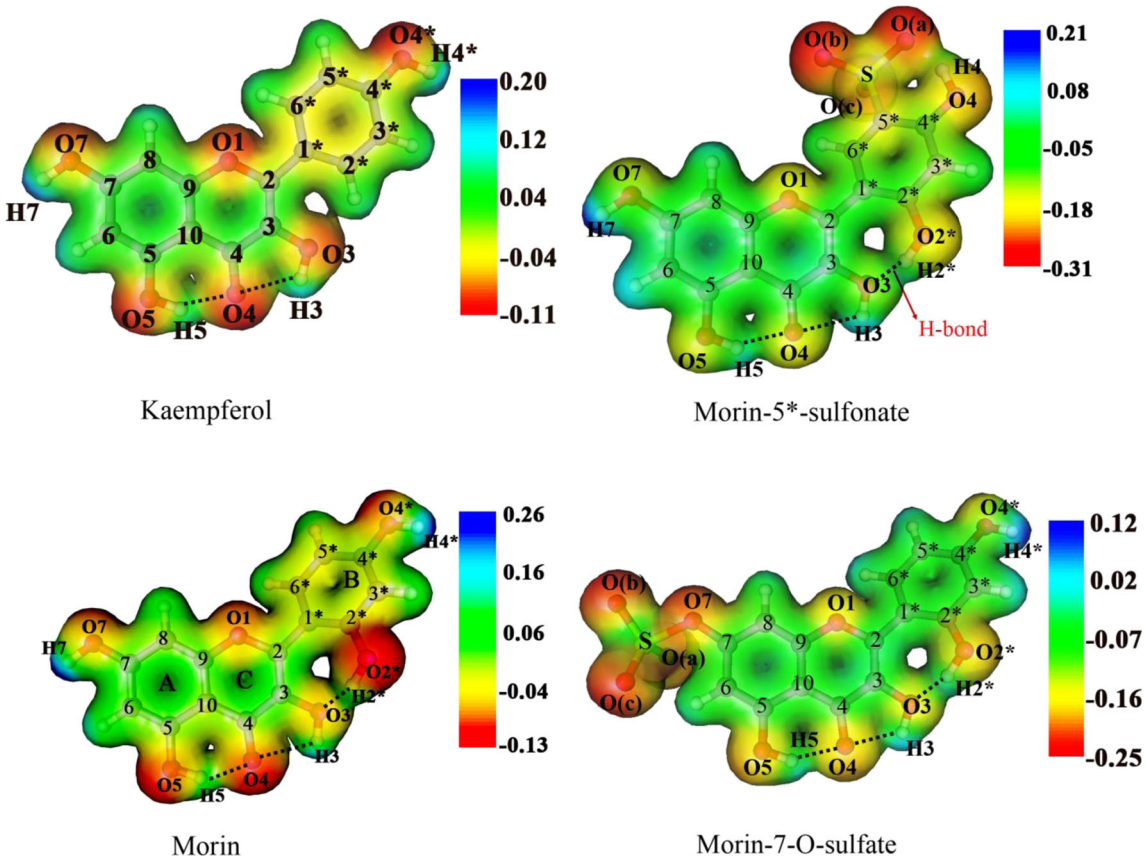

Fig. 2 Optimized geometries in aqueous solution of four kaempferol-based compounds under study

Solvation energies of kaempferol-based compounds

The total Gibbs energies of solvation ($\Delta G_{solv,tot}$) with electrostatic contributions ($\Delta G_{solv,es}$) and non-electrostatic contributions ($\Delta G_{solv,non\text{-}es}$) are shown in Table 1 for all kaempferol-based compounds in three media, i.e., water, methanol, and carbon tetrachloride. Following the values of $\Delta G_{solv,tot}$ in water (kcal mol^{-1}), the preference of compounds to be hydrated decreases in the order: morin-5*-sulfonate > morin-7-O-sulfate >> morin > kaempferol. The solute-solvent interaction is strongest in morin-5*-sulfonate followed by morin-7-O-sulfate, being in agreement with their superior solubility in water. The lower degree of hydration for morin-7-O-sulfate is partly due to the lack of O7-H7 group. For kaempferol and morin, the hydrophilicity basically increases with the number of OH group. The non-electrostatic contributions for all compounds in water are quite small, with $\Delta G_{solv,non\text{-}es}$ lying in the range of 4.07–6.86 kcal mol^{-1}. The positive sign of $\Delta G_{solv,non\text{-}es}$ in water suggests that the non-electrostatic interactions favor the desolvation. However, for every compound, the hydration process is dominated by the electrostatic contributions. When changing the medium from water to carbon tetrachloride, the sign of $\Delta G_{solv,non\text{-}es}$ remain positive but the values are decreased. Therefore, the desolvating effect caused by non-electrostatic interactions in carbon tetrachloride is not as large as it is in water. The electrostatic contributions for all compounds in carbon tetrachloride are obviously smaller than those in water. The preference of compound to be solvated by carbon tetrachloride decreases in the order: morin-5*-sulfonate > morin-7-O-sulfate >> morin > kaempferol, which is the same order as in the case of water. However, the overall solute-solvent interactions in carbon tetrachloride are obviously weaker than those in water. Among all solvents tested, methanol shows the strongest preference to solvate every kaempferol-based compound. The electrostatic contributions for all compounds in methanol are slightly smaller than those in water. However, for morin-5*-sulfonate and morin-7-O-sulfate in methanol, the desolvating effect caused by non-electrostatic contributions is effectively minimized, yielding small positive values of $\Delta G_{solv,non\text{-}es}$ ($\approx$ 0.4 kcal mol^{-1}). Furthermore, for morin and kaempferol in methanol, the sign of $\Delta G_{solv,non\text{-}es}$ becomes negative, indicating that the non-electrostatic interactions in this case distinctively favor the solvation. In summary, on the basis of the total Gibbs energy of solvation, the solubility of any kaempferol-based compound in this work is varied with the type of solvent as: methanol > water >> carbon tetrachloride. In any solvent tested, the solubility of compound decreases in the order: morin-5*-sulfonate > morin-7-O-sulfate >> morin > kaempferol.

Thermodynamic aspects of HAT and stability of oxyradical products

Thermodynamic parameters for the transfer of each hydroxyl H atom from kaempferol-based compounds to ·OH in aqueous solution are summarized in Table 2. With the negative values of enthalpy (ΔH_r) and the positive values of entropy (ΔS_r), all 18 HAT reactions are exothermic and spontaneous at 298 K. The values of ΔS_r are so small (2.68–6.04 cal mol^{-1} K^{-1}) that all HAT reactions are regarded as the enthalpy-driven processes. The highly negative value of ΔE_r is mainly due to the fact that the oxyradical product has greater stability than the initiator ·OH. It is worth remarking that conversion of a high-energy radical into another low-energy radical is always desirable as the high-energy radical is more harmful to the biomolecules exposed to it. The likelihood of the hydroxyl H atom being abstracted by ·OH increases in the following order: kaempferol (O4*-H4*, −26.7) < morin-5*-sulfonate (O3-H3, −27.6) < morin (O3-H3, −30.5) < morin-7-O-sulfate (O3-H3, −32.9), with the label and number in each parenthesis indicating the most preferable site for HAT and the corresponding Gibbs energy of HAT under hydration (ΔG_r: kcal mol^{-1}), respectively. Several previous works have claimed that morin is more potent in scavenging either ·OH or ·DPPH (1,1-diphenyl-2-picrylhydrazyl radical) than kaempferol [6, 8, 30], being in agreement with the reaction potentials of both compounds predicted by the ΔG_r values. It has been reported that morin-5*-sulfonate has higher scavenging activity toward ·DPPH than morin [4].

Table 1 Total Gibbs energies of solvation ($\Delta G_{solv,tot}$) at 298 K with non-electrostatic contributions ($\Delta G_{solv,non\text{-}es}$) and electrostatic contributions ($\Delta G_{solv,es}$) for kaempferol-based compounds in water (H_2O), carbon tetrachloride (CCl_4), and methanol (CH_3OH). All data are based on PCM-DFT calculations at the CAM-B3LYP/6–311++G(d,p) level

	H_2O (dielectric constant = 78.39)			CCl_4 (dielectric constant = 2.228)			CH_3OH (dielectric constant = 32.63)		
	$\Delta G_{solv,tot}$[a]	$\Delta G_{solv,non\text{-}es}$[a]	$\Delta G_{solv,es}$[a]	$\Delta G_{solv,tot}$[a]	$\Delta G_{solv,non\text{-}es}$[a]	$\Delta G_{solv,es}$[a]	$\Delta G_{solv,tot}$[a]	$\Delta G_{solv,non\text{-}es}$[a]	$\Delta G_{solv,es}$[a]
Kaempferol	− 17.36	4.07	− 21.43	− 1.32	2.60	− 3.93	− 21.31	− 0.92	− 20.39
Morin	− 18.66	4.34	− 23.00	− 1.37	2.90	− 4.26	− 22.68	− 0.81	− 21.87
Morin-5*-sulfonate	− 60.95	6.73	− 67.68	− 21.42	5.01	− 26.43	− 65.19	0.44	− 65.63
Morin-7-O-sulfate	− 53.35	6.86	− 60.21	− 18.95	5.04	− 23.99	− 57.92	0.42	− 58.34

[a] All values are in units of kcal mol^{-1}

Table 2 Binding energies and thermodynamic parameters at 298 K for the transfer of H atom from different OH groups of each kaempferol-based compound to ·OH in aqueous solution. All data are based on PCM-DFT calculations at the CAM-B3LYP/6–311++G(d,p) level

Compound	Reactive group	Binding energy[a]	Thermodynamic parameters of HAT[(b)]				Reaction potential ranking[g]
			ΔE_r[c]	ΔH_r[d]	ΔS_r[e]	ΔG_r[f]	
Kaempferol	O3-H3	− 11.8	− 25.2 (0.78)	− 25.0 (0.85)	3.69 (1.01)	− 26.1 (0.61)	6
	O5-H5	− 5.18	− 10.1 (15.9)	− 9.74 (16.1)	5.23 (2.55)	− 11.3 (15.4)	16
	O7-H7	− 8.81	− 20.6 (5.38)	− 20.4 (5.42)	3.36 (0.67)	− 21.4 (5.27)	9
	O4*-H4*	− 10.2	− 26.0 (0)	− 25.9 (0)	2.68 (0)	− 26.7 (0)	5
Morin	O3-H3	− 5.50	− 29.3 (0)	− 29.1 (0)	4.70 (1.34)	− 30.5 (0)	2
	O5-H5	− 0.58	− 10.1 (19.2)	− 9.66 (19.4)	5.50 (2.15)	− 11.3 (19.2)	16
	O7-H7	− 9.97	− 20.0 (9.30)	− 19.8 (9.30)	3.36 (0)	− 20.8 (9.70)	10
	O2*-H2*	− 7.27	− 16.1 (13.2)	− 15.6 (13.5)	6.04 (2.68)	− 17.4 (13.1)	13
	O4*-H4*	− 3.71	− 22.8 (6.50)	− 22.6 (6.50)	3.36 (0)	− 23.6 (6.90)	7
Morin-5*-sulfonate	O3-H3	− 12.9	− 26.3 (0)	− 26.1 (0)	5.03 (1.68)	− 27.6 (0)	4
	O5-H5	− 5.83	− 7.69 (18.6)	− 7.26 (18.8)	5.64 (2.28)	− 8.94 (18.7)	17
	O7-H7	− 0.55	− 17.4 (8.90)	− 17.2 (8.90)	3.36 (0)	− 18.2 (9.40)	11
	O2*-H2*	− 16.1	− 13.9 (12.4)	− 13.4 (12.7)	6.04 (2.68)	− 15.2 (12.4)	15
	O4*-H4*	− 0.37	− 21.2 (5.10)	− 21.0 (5.10)	3.36 (0)	− 22.0 (5.60)	8
Morin-7-O-sulfate	O3-H3	− 14.0	− 31.5 (0)	− 31.3 (0)	5.37 (1.68)	− 32.9 (0)	1
	O5-H5	− 5.87	− 14.2 (17.3)	− 13.9 (17.4)	5.70 (2.01)	− 15.6 (17.4)	14
	O2*-H2*	− 19.6	− 16.6 (15.0)	− 16.1 (15.2)	6.04 (2.35)	− 17.9 (15.1)	12
	O4*-H4*	− 13.8	− 27.9 (3.65)	− 27.7 (3.61)	3.69 (0)	− 28.8 (4.14)	3

[a] Energy (kcal mol^{-1}) involved with the binding of ·OH to OH group of kaempferol-based compound at ground state

[b] All numbers in parentheses are the values relative to the minimum

[c] Potential energy (kcal mol^{-1})

[d] Enthalpy (kcal mol^{-1})

[e] Entropy (cal mol^{-1} K^{-1})

[f] The Gibbs energy (kcal mol^{-1})

[g] Ranking is based on the ΔG_r values of all 18 reactions

The thermodynamic data for the HAT reactions of kaempferol are quite unique as its O3-H3 and O4*-H4* groups display very similar ΔG_r values of − 26.1 kcal mol^{-1} and − 26.7 kcal mol^{-1}, respectively. Thus, it would be fair to say that the H atoms in both OH groups of kaempferol are comparably preferred by ·OH. Previously, the close-lying pK_a values of kaempferol have been experimentally detected [31]. Some previous studies have also reported that the bond dissociation enthalpy of O4*-H4* in kaempferol is very close to that of O3-H3 [32, 33]. The previous work has proposed that the presence of O4*-H4* is an essential element for the potent ·OH-scavenging activity of kaempferol [34]. Excluding kaempferol, O3-H3 is obviously the most preferable group for the H-atom abstraction, being in accordance with previous studies [34–36]. This is mainly due to the fact that O3-radical has greater stability than the respective O4*-radical. The optimized geometries of 18 oxyradical products are shown in Supplementary Materials (Fig. S1-S4). The marked stability of O3-radicals of morin and its derivatives is ascribed to the presence of an intramolecular hydrogen bond between H2* and O3 (the unpaired-electron center). Correspondingly, owing to the lack of such a hydrogen bond, O3-radical of kaempferol cannot be stabilized as effectively as that of morin or morin derivatives. Following the electrostatic potential maps shown in Supplementary Materials (Fig. S1-S4) for each O4*-radical, the electron-donating effect of O2*-H2* (not present in kaempferol) introduces excess negative charges to ring B, decreasing charge stability. On the other hand, for O3-radicals of either morin or its derivatives, the formation of O3···H2* (a hydrogen bond) effectively reduces the accumulation of electrons on the unpaired-electron center (O3), hence promoting charge stability. The O3···H2* distances in all O3-radicals are similarly close to 1.50 Å, being shorter than the sum of the van der Waals radii of H and O atoms (2.7 Å) [37] but still longer than the adjacent covalent bond H2*-O2* (≈ 1.02 Å). The angle O3···H2*-O2* varies between 165° and 167° whereas all O3-O2* interatomic distances are close to 2.48 Å. Based on these

structural data, O3···H2* in each O3-radical could be regarded as a moderate hydrogen bond with primary electrostatic contribution [38]. The Coulomb attractive forces (e^2 Å^{-2}) between O3 and H2* in all O3-radicals based on the NBO atomic charge data can be sorted as morin-7-O-sulfate (−0.136) > morin (−0.135) > morin-5*-sulfonate (−0.133). It is noteworthy to remind that in the case of kaempferol, O3···H2* cannot be formed due to the absence of O2*-H2*. According to the NBO analysis, the O3···H2* interaction within each O3-radical can be described in terms of donor-acceptor orbital interaction between the valence-shell nonbonding orbital of O3 [represented by NB(O3)] and the anti-bonding orbital of the covalent bond O2*-H2* [represented by BD*(O2*-H2*)]. The energy of interaction NB(O3)-BD*(O2*-H2*) (kcal mol^{-1}), which is a measure of the strength of O3···H2 in each O3-radical decreases in the following order: morin-7-O-sulfate (26.43) > morin (25.92) > morin-5*-sulfonate (25.75). Clearly, O3···H2* in O3-radical of morin can be strengthened and weakened by the addition of sulfate and sulfonate groups, respectively. Basically, the weakening of O3···H2* lowers the charge stability of O3-radical, and this in turn reduces the likelihood of such a radical to be formed. This principle satisfactorily accounts for the decrease (increase) in the reaction potential of O3-H3 upon the addition of sulfonate group (sulfate group) to morin.

For every compound tested, the HAT reaction at O5-H5 is found to be least favorable as it gives rise to the least stable oxyradical product, i.e., O5-radical. This result is in line with the previous study in which O5-H5 has been reported as being the least acidic OH group in kaempferol and quercetin [39, 40]. Finding the way to increase the reaction preference at this particular OH group would be a challenge. As seen in the structures of O5-radicals (Supplementary Materials, Fig. S1-S4), after the removal of H5, the negative charges on O4 (the carbonyl O atom) and O5 (the unpaired-electron center) are much exposed to each other, definitely causing an electrostatic repulsion between both O atoms. Evidently, the O4-O5 repulsion widens the bond angles O4-C4-C10 and O5-C5-C10 in O5-radicals with respect to the corresponding angles in the other oxyradicals. For more information on these bond angles, O4-C4-C10 (O5-radicals: 128°–129°; other oxyradicals: 121°–126°) and O5-C5-C10 (O5-radicals: 122°–123°; other oxyradicals: 119°–121°). Given that the O4-O5 repulsion electronically destabilizes the geometry of O5-radical, it is useful to know how much the strength of such a repulsion is affected by the substituent. The O4-O5 repulsive forces (e^2 Å^{-2}) in all O5-radicals can be sorted as morin-7-O-sulfate (4.025×10^{-2}) < morin (4.062×10^{-2}) < morin-5*-sulfonate (4.083×10^{-2}) < kaempferol (4.204×10^{-2}). The greatest ability to counteract the O4-O5 repulsion in O5-radical therefore belongs to the 7-O-sulfate group—thanks to its prominent electron-withdrawing ability.

Kinetic aspects of HAT at individual OH groups

With the optimized TS geometries in hand, the corresponding intrinsic reaction coordinate (IRC) paths were subsequently determined. As an example, the IRC paths for the attack of ·OH at O3-H3 in different compounds are displayed in Fig. 3. The end points of each IRC path were further optimized to yield the pre-reactive complex (·OH hydrogen-bonded to the kaempferol-based molecule) and post-reactive complex (H_2O hydrogen-bonded to the oxyradical product). The theoretical pathway of HAT upon the attack of ·OH can be written as

$$\begin{aligned} &\mathrm{R{-}OH} \\ &+ \cdot\mathrm{OH} \rightarrow \mathrm{R{-}OH\cdots OH} \rightarrow \mathrm{TS} \rightarrow \mathrm{R{-}O\cdots HOH} \rightarrow \mathrm{R{-}O} \\ &+ \mathrm{H_2O}, \end{aligned} \tag{5}$$

where R-OH···OH and R-O···HOH represent the pre-reactive and post-reactive complexes, respectively. Taking morin-5*-sulfonate as an example, the transfer of H3 from O3-H3 to ·OH following the above pathway can be represented by the diagram in Fig. 4. Table 2 includes the binding energies (ΔE_{bin}), each of which is referred to as the energy released from the system upon the binding of ·OH to the kaempferol-based compound. The magnitude of ΔE_{bind} therefore reflects the strength of hydrogen bonding between both reactants. Based on the ΔE_{bind} data, the most favorable binding site for ·OH in each compound is given by kaempferol (O3-H3), morin (O7-H7), morin-5*-sulfonate (O2*-H2*), and morin-7-O-sulfate (O2*-H2*). The preference of a given OH group to bind to ·OH varies with the choice of compound as follows:

- O3-H3: morin-7-O-sulfate > morin-5*-sulfonate > kaempferol >> morin
- O7-H7: morin > kaempferol >> morin-5*-sulfonate
- O2*-H2*: morin-7-O-sulfate > morin-5*-sulfonate >> morin
- O4*-H4*: morin-7-O-sulfate > kaempferol >> morin > morin-5*-sulfonate

Overall, the hydrogen bonding between O* in ·OH and the hydroxyl H atom of compound is obviously favorable in morin-7-O-sulfate. Nevertheless, there would be no explicit relationship between ΔE_{bind} and the reaction potential described earlier because the likelihood of the H atom in a kaempferol-based molecule being successfully abstracted by the incoming ·OH depends primarily on the relative stability

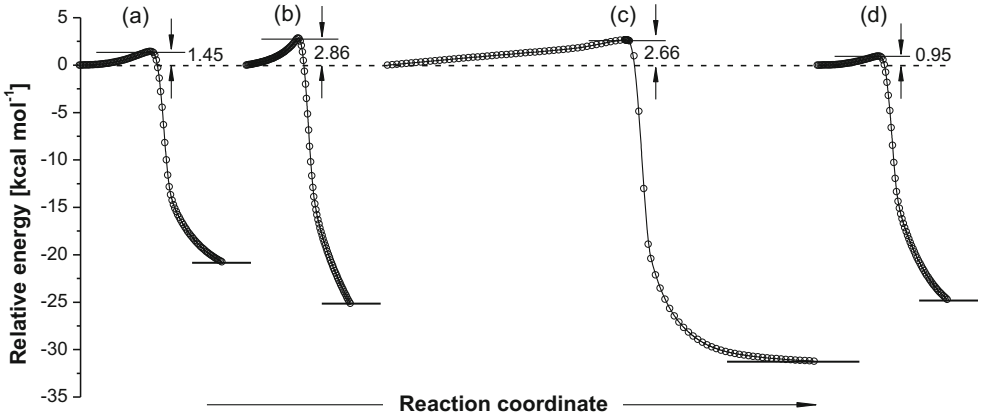

Fig. 3 Energy profiles obtained by intrinsic reaction coordinate (IRC) calculations for the attack of ·OH at O3-H3 of **a** kaempferol, **b** morin, **c** morin-5*-sulfonate, and **d** morin-7-O-sulfate in aqueous solution at 298 K. The maximum in each profile corresponds to transition state (TS). The initial and final states are the pre-reactive complex and the post-reactive complex, respectively

of the oxyradical product rather than the strength of interactions between the reactants.

The essential kinetic data for all possible HAT reactions of kaempferol-based compounds initiated by ·OH in aqueous solution are presented in Table 3. The orders of magnitude of most rate constants obtained in this work are in the range for typical ·OH reactions (~10^9–10^{10} M^{-1} s^{-1}) [7]. The four highest rate constants (k) of all reactions can be sorted as morin-5*-sulfonate ($k_{O4*-H4*}$) > morin ($k_{O2*-H2*}$) > morin-5*-sulfonate (k_{O5-H5}) > morin (k_{O3-H3}). Morin-5*-sulfonate and morin therefore exhibit prominent kinetic reactivity toward ·OH. The dependence of reaction rate on the location of OH group in each compound is given as follows:

- Kaempferol: O3-H3 > O7-H7 > O5-H5 > O4*-H4*
- Morin: O2*-H2* > O3-H3 > O4*-H4* > O7-H7

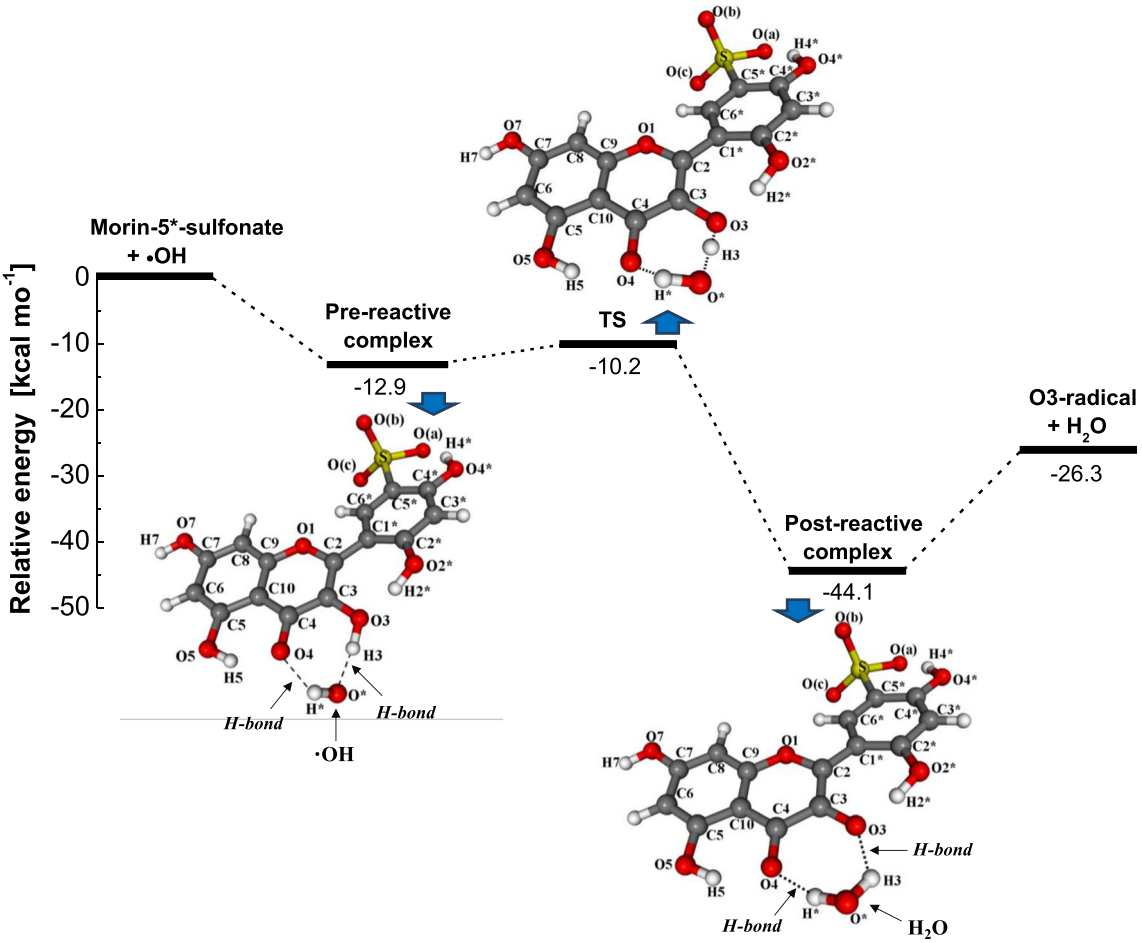

Fig. 4 Energy diagram for HAT from O3-H3 of morin-5*-sulfonate to ·OH. The optimized geometries of TS, pre-reactive complex, and post-reactive complex are all included

Table 3 Kinetic parameters at 298 K for the transfer of H atom from different OH groups of each kaempferol-based compound to ·OH in aqueous solution. All data are based on PCM-DFT calculations at the CAM-B3LYP/6–311++G(d,p) level

Reactive group	Compound	ν_i[a]	κ[b]	A[c]	$E^{\ddagger}$[d]	k[e]	k/k_{ref}	Kinetic effect of substituent	Reaction rate ranking[f]
O3-H3	Kaempferol	663.2	1.43	1.65×10^{11}	1.45	1.42×10^{10}	1	Reference	6
	Morin	1753.6	3.99	3.99×10^{12}	2.86	3.20×10^{10}	2.25	Activate	4
	Morin-5*-sulfonate	186.3	1.03	4.00×10^{10}	2.66	4.49×10^{8}	0.03	Deactivate	13
	Morin- 7-O-sulfate	667.8	1.43	1.10×10^{11}	0.95	2.22×10^{10}	1.55	Activate	5
O5-H5	Kaempferol	1420.0	2.96	3.48×10^{10}	3.83	5.43×10^{7}	1	Reference	16
	Morin	1094.3	2.16	8.64×10^{11}	3.11	4.54×10^{9}	83.6	Activate	10
	Morin-5*-sulfonate	1033.0	2.04	3.60×10^{11}	1.30	4.02×10^{10}	740	Activate	3
	Morin- 7-O-sulfate	825.5	1.66	3.13×10^{10}	2.91	2.31×10^{8}	4.25	Activate	14
O7-H7	Kaempferol	594.8	1.34	1.68×10^{10}	0.41	8.34×10^{9}	1	Reference	9
	Morin	119.8	1.01	3.22×10^{10}	0.73	9.40×10^{9}	1.13	Activate	8
	Morin-5*-sulfonate	82.0	1.01	1.26×10^{10}	0.77	3.44×10^{9}	0.41	Deactivate	11
O2*-H2*	Morin	474.2	1.22	4.18×10^{11}	1.27	4.90×10^{10}	1	Reference	2
	Morin-5*-sulfonate	691.6	1.46	9.72×10^{10}	5.42	1.04×10^{7}	2.12×10^{-4}	Deactivate	18
	Morin-7-O-sulfate	858.2	1.72	8.78×10^{10}	3.68	1.76×10^{8}	3.59×10^{-3}	Deactivate	15
O4*-H4*	Kaempferol	84.2	1.01	2.05×10^{9}	2.35	3.88×10^{7}	1	Reference	17
	Morin	215.0	1.04	4.70×10^{10}	0.79	1.24×10^{10}	319.6	Activate	7
	Morin-5*-sulfonate	915.4	1.81	5.51×10^{13}	1.55	4.02×10^{12}	1.04×10^{5}	Activate	1
	Morin-7-O-sulfate	939.6	1.86	1.97×10^{10}	1.95	7.34×10^{8}	18.9	Activate	12

[a] Imaginary part of vibrational frequency of TS geometry (cm^{-1})

[b] The Wigner transmission coefficient

[c] Pre-exponential factor ($dm^3\ mol^{-1}\ s^{-1}$)

[d] Activation energy (kcal mol^{-1})

[e] Rate constant ($dm^3\ mol^{-1}\ s^{-1}$)

[f] Ranking is based on the k values of all 18 reactions

- Morin-5*-sulfonate: O4*-H4* > O5-H5 > O7-H7 > O3-H3 > O2*-H2*
- Morin-7-O-sulfate: O3-H3 > O4* H4* > O5-H5 > O2*-H2*

It is noted that except for morin-5*-sulfonate, the kinetic reactivity of O3-H3 is markedly high in most compounds.

In order to appropriately characterize the effect of substituents on the HAT rate, the kinetic reactivity of the individual OH groups are described as follows:

1. C3-Hydroxyl group (O3-H3). O3-H3 is found to be the most kinetically reactive group in two compounds (kaempferol and morin-7-O-sulfate) and the second most reactive group in one compound (morin). The prominent kinetic reactivity toward ·OH of this particular OH group on ring C, interestingly, coincides with its markedly high thermodynamic reaction potential as mentioned earlier. The kinetic reactivity of O3-H3 decreases in the order morin > morin-7-O-sulfate > kaempferol (reference) > morin-5*-sulfonate. Compared to kaempferol (the parent compound), the activating effect on O3-H3 is resulted in every case except morin-5*-sulfonate. The activation energy for the attack of ·OH at O3-H3 decreases as morin > morin-5*-sulfonate > kaempferol (reference) > morin-7-O-sulfate. Given that the activation energy ($E^{\ddagger}$) of morin (2.86 kcal mol^{-1}) is almost twice as high as that of kaempferol (1.45 kcal mol^{-1}), the highest reaction rate at O3-H3 for morin is principally attributed to the massive pre-exponential factor, caused by either the large partition function of TS relative to the pre-reactive complex or the exceptionally high imaginary vibrational frequency of TS. This case simply demonstrates that the kinetic reactivity cannot be judged alone by the value of activation energy according to the TS theory.

Following the TS structure analysis, O*···H3 (with O* being the O atom in ·OH), a hydrogen bond which plays a key role in attracting ·OH to the reactive O3-H3 group, becomes strongest in the case of morin. For more details, the O*-H3 attractive force (e^2 Å^{-2}) within the optimized TS structure decreases in the sequence: morin (− 0.159) > morin-7-O-sulfate (− 0.123) > kaempferol (− 0.108) > morin-5*-sulfonate (− 0.057). Correspondingly, the strength of O*···H3 decreases in the same sequence as the imaginary vibrational frequency of

the TS geometry. Now, let us consider the structural effect on the TS stability, the reactive-site geometry formed by following seven atoms: C4, O4, H*, O*, H3, O3, and C3 in the TS structure of kaempferol (Fig. 5a) displays an outstanding degree of planarity, implying high stability and hence low $E^{\ddagger}$. Such a seven-membered reactive site is organized so well that it is almost coplanar with the entire kaempferol molecule. As seen in Fig. 5b, the observation on the HOMO plot for the TS structure of kaempferol reveals a significant degree of π-electron delocalization over the three O atoms at the reactive site—such a feature is not found in the case of morin. According to the NBO analysis, a relatively strong hydrogen bond such as O4···H* plays a key role in organizing the reactive-site geometry of kaempferol. For more information, the O4-H* attractive forces (e^2 Å^{-2}) within TS are in the order: kaempferol (− 0.085) > morin-7-O-sulfate (− 0.078) > morin and morin-5*-sulfonate (none). Although O4···H* in the TS of morin-7-O-sulfate is not as strong as that in the TS of kaempferol, the electronic effect of the sulfate group in the former give rises to the exceptionally uniform charge distribution over the whole three-ring skeleton (Supplementary Materials, Fig. S5), being responsible for the lowest $E^{\ddagger}$ of 0.95 kcal mol^{-1}. For the TS structure of morin or morin-5*-sulfonate, the O4-H* attractive force is replaced by the O4-O* repulsive force (morin: 0.063 e^2 Å^{-2}; morin-5*-sulfonate: 0.055 e^2 Å^{-2}), hence increasing the value of $E^{\ddagger}$. It is noted that the stronger the O4-O* repulsive force is, the higher the $E^{\ddagger}$ value will become. The region in which the O4-O* repulsion is active in the TS structure of morin is illustrated in Fig. 5a for clarification.

2. C5-Hydroxyl group (O5-H5). The rate constant for the attack of ·OH at O5-H5 on ring A can be increased from the reference value of kaempferol by any choice of substituents attempted herein. The most kinetically enhanced reaction at O5-H5 belongs to morin-5*-sulfonate. It is noted that the C5*-sulfonate group somehow affects the reactivity of O5-H5 in the opposite way to what it does to the reactivity of O3-H3 as mentioned earlier.

As seen in Table 3, the highest HAT rate at O5-H5 of morin-5*-sulfonate is mainly due to the remarkably low $E^{\ddagger}$ value (1.30 kcal mol^{-1}). Let us consider the TS structure formed upon the radical attack at O5-H5 of morin-5*-sulfonate (Fig. 6a). The reactive-site geometry built up of the following eight atoms: O5, C5, C10, C4, O4, H*, O*, and H5 is almost planar. The HOMO plot included reveals the presence of π-electron delocalization over the segment O5···H*···O*, indicating a favorable orbital interaction between O5 and O* at the reactive site. The electron density over the eight-membered reactive site in the TS structure of morin-5*-sulfonate as seen in Fig. S6 (Supplementary Materials) appears more homogeneous than the same site in the corresponding

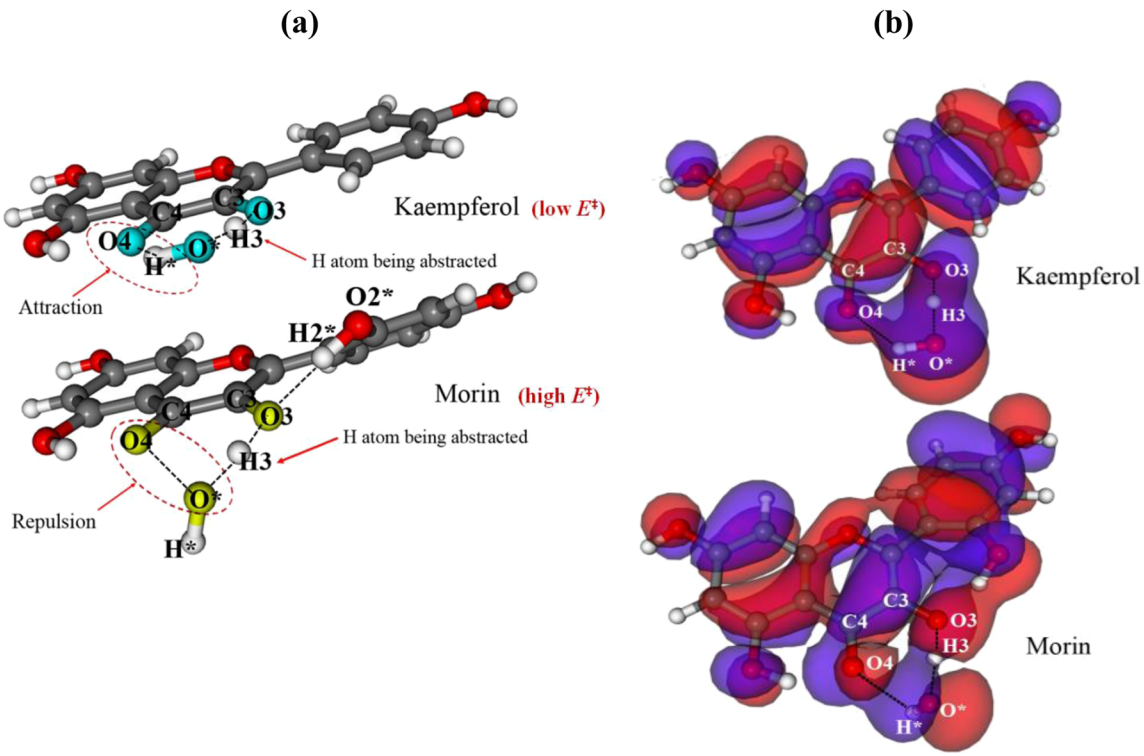

Fig. 5 **a** Formation of seven-membered reactive site in the TS structures formed upon the attack of ·OH at O3-H3 of kaempferol and morin. **b** Spatial distribution of the HOMOs of the TS structures formed upon the attack of ·OH at O3-H3 of kaempferol and morin

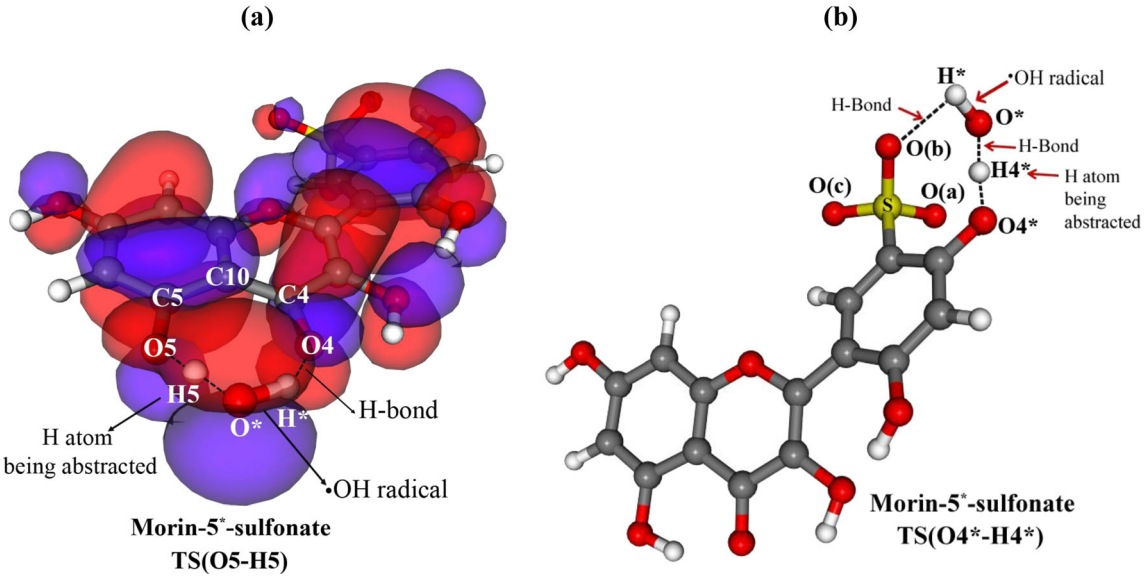

Fig. 6 **a** Formation of eight-membered reactive site in the TS structure formed upon the attack of ·OH at O5-H5 of morin-5*-sulfonate. The spatial distribution of HOMO is included. **b** The TS structure formed upon the attack of ·OH at O4*-H4* of morin-5*-sulfonate

TS structures of the other compounds. The presence of the C5*-sulfonate group on ring B is so effective in reducing the excess negative charges on several O atoms such as O1, O3, O4, O5, and O7, rendering the charge density on the chromone moiety highly homogeneous. The charge stability of O* (the unpaired-electron center of ·OH) in this case should be remarkably high. On the other hand, for the TS structures of either kaempferol or morin (Supplementary Materials, Fig. S6), the electron density on O* is noticeably higher than that on either O4 or O5. The most effective electron distribution over the reactive site of the TS structure of morin-5*-sulfonate essentially accounts for its lowest $E^{\ddagger}$. When changing from kaempferol to morin-5*-sulfonate, the fractions of electrons (in %) populated on the O atoms and the C atoms in the chromone moiety of the TS structure are reduced from 6% to 4% and from 4% to 3%, respectively. This result ensures a long-range effect of the sulfonate group on the distribution of negative charges on the O atoms within the chromone moiety. In the TS structure of morin-7-O-sulfate (Supplementary Materials, Fig. S6), the electron density on O* appears quite similar to that on either O4 or O5; however, the degree of charge homogeneity is not as obvious as that in the TS structure of morin-5*-sulfonate. Consequently, the charge stability of O* in the TS structure of morin-7-O-sulfate is expected to be slightly lower than that in the TS structure of morin-5*-sulfonate.

Another interesting feature found in the TS structure is the formation of an intermolecular hydrogen bond O4···H* (see Fig. 6a), which plays a key role in confining the orientation of ·OH within the reactive site. The O4-H* attractive force (e^2 Å^{-2}) in the TS structure is varied with the type of compound as morin-7-O-sulfate (− 0.1058) > morin-5*-sulfonate (− 0.1009) > morin (− 0.0997) > kaempferol (− 0.0995). For morin-7-O-sulfate, both the strongest O4···H* and the marked charge stability of O* within the TS structure account for its low $E^{\ddagger}$.

3. C7-Hydroxyl group (O7-H7). Taking kaempferol as a reference, the kinetic reactivity of O7-H7 on ring A is found to be activated and deactivated in morin and morin-5*-sulfonate, respectively. In the TS structure of morin-5*-sulfonate (Supplementary Materials, Fig. S7), the electron density over the chromone moiety is strikingly low because of the long-range electron-withdrawing ability of the C5*-sulfonate group located on ring B. According to the electron population analysis, the fraction of electrons (in %) populated on the six C atoms on ring A of the TS structure decreases in the order: kaempferol (22.7%) > morin (21.6%) > morin-5*-sulfonate (17.4%). The distinctive reduction in the electron density over the chromone moiety not only promotes the $E^{\ddagger}$ value but also decreases the total partition function of the TS structure of morin-5*-sulfonate. In the case of morin, the massive pre-exponential factor is a key to the highest kinetic reactivity of its O7-H7 toward the attack of ·OH. The O*-H7 attractive force (e^2 Å^{-2}) in the TS geometry decreases in the order morin (− 0.170) > kaempferol (− 0.168) > morin-5*-sulfonate (− 0.150). The pre-exponential factor is significantly correlated to the strength of O*···H7 in the TS structure.
4. C2*-Hydroxyl group (O2*-H2*). Due to the lack of O2*-H2* in kaempferol, the kinetic reactivity of this OH group in morin-5*-sulfonate or morin-7-O-sulfate needs to be compared with morin. The addition of either sulfonate or sulfate groups to morin drastically decreases the rate of HAT at O2*-H2*. Compared to morin, the pre-

exponential factor is reduced by a factor of 4.3 and 4.8 in morin-5*-sulfonate and morin-7-O-sulfate, respectively. However, the substantial decrease in the rate constant value upon the addition of substituents to morin is primarily connected to the increase in $E^{\ddagger}$. The attack of ·OH at O2*-H2* of morin-5*-sulfonate, with the highest $E^{\ddagger}$ of 5.42 kcal mol^{-1}, is the slowest of all 18 reactions under study. The optimized TS structures formed upon the HAT reactions at O2*-H2* of morin and its two derivatives are depicted in Supplementary Materials, Fig. S8. The kinetics of HAT at O2*-H2* is significantly affected by the presence of O*···H2*—a hydrogen bond which attracts ·OH toward the reactive O2*-H2* group. The O*-H2* attractive force (e^2 Å^{-2}) in the TS structure decreases in the order: morin-7-O-sulfate (− 0.256) > morin (− 0.249) > morin-5*-sulfonate (− 0.244). Furthermore, a careful observation on the TS structures (Supplementary Materials, Fig. S8) reveals that while ·OH approaches the reactive O2*-H2* group on ring B, its O atom (denoted by O*) will encounter an electrostatic repulsion against O3 on ring C. In terms of kinetics, such a repulsion is definitely an obstacle to the radical attack at O2*-H2*. The O*-O3 repulsive forces (e^2 Å^{-2}) in the TS structures are in the order morin-5*-sulfonate (0.0870) > morin-7-O-sulfate (0.0841) > morin (0.0837). The strongest O*-O3 repulsion is the TS structure of morin-5*-sulfonate basically emerges from the highest negative charge on O3. For more information, the amount of negative charge on O3 in the TS structure decreases in the order: morin-5*-sulfonate (− 0.640e) > morin-7-O-sulfate (− 0.638e) > morin (− 0.632e). Allowing for both the weakest O*-H2* attraction and the strongest O*-O3 repulsion in the TS structure, the attack of ·OH at O2*-H2* of morin-5*-sulfonate should be most considerably retarded. For morin, the highest rate of HAT at O2*-H2* is consistent with the weakest O*-O3 repulsion within the corresponding TS structure.

5. C4*-Hydroxyl group (O4*-H4*). Among all OH groups in kaempferol, O4*-H4* on ring B is least kinetically reactive toward the attack of ·OH. It is worth noting that the highest thermodynamic reaction potential of this OH group in kaempferol as mentioned earlier could be opposed by its lowest kinetic reactivity to some extent. On the other hand, O3-H3 in kaempferol, with the thermodynamic reaction potential being comparable to O4*-H4*, is much more kinetically reactive to ·OH. The rate constant for the attack of ·OH at O3-H3 in kaempferol is 366 times as large as that for the corresponding reaction at O4*-H4* in the same compound. Allowing for this fact, it would be useful to know whether the kinetic reactivity of O4*-H4* can be promoted by the effect of substituent. Based on the rate constant values, the kinetic reactivity of O4*-H4* toward the attack of ·OH decreases in the following sequence: morin-5*-sulfonate >> morin >> morin-7-O-sulfate > kaempferol (reference). The kinetic enhancement with respect to kaempferol is therefore resulted in all cases. By merely adding O2*-H2* to ring B of kaempferol (as in the case of morin), the rate constant can be increased by a factor of 320. There is a correlation between the strength of O*···H4* in the TS structure and the value of imaginary vibrational frequency since the presence of strong O*···H4* normally reduces the electron density over the adjacent O4*-H4*. For further information, the O*-H4* attractive force (e^2 Å^{-2}) decreases in the order morin-7-O-sulfate (− 0.219) > morin-5*-sulfonate (− 0.199) > morin (− 0.183) > kaempferol (− 0.123). The attack of ·OH at O4*-H4* of morin-5*-sulfonate is regarded as the fastest of all 18 reactions tested. The exceptionally large pre-exponential factor of morin-5*-sulfonate has a great contribution to its highest rate constant. As depicted in Fig. 6b, hydrogen bonding between the H* atom in ·OH and the sulfonate O atom (O(b)) assists in the incorporation of ·OH into the reactive site, being in accordance with the massive pre-exponential factor.

Considering the electrostatic potential maps shown in Fig. S9 (Supplementary Materials), the negative charges in the TS structure of kaempferol are populated more intensely on ring B than the other rings, whereas the negative charges in the TS structure of morin are distributed more uniformly throughout the three-ring skeleton. This observation agrees with the highest and lowest $E^{\ddagger}$ values for the reactions at O4*-H4* of kaempferol and morin, respectively. For the TS structure of morin-7-O-sulfate, the inductive effect of the sulfate group particularly reduces the electron density on the chromone moiety, making the $E^{\ddagger}$ value of morin-7-O-sulfate not much different from that of kaempferol. For the TS structure of morin-5*-sulfonate, the electron density on ring A is slightly lower than that on the other rings; therefore, this could be the main reason for morin-5*-sulfonate to have higher $E^{\ddagger}$ than morin.

Conclusions

Following the DFT-based thermodynamic data obtained in this work, the most and the least preferable sites for the attack of ·OH are assigned to O3-H3 in morin-7-O-sulfate and O5-H5 in morin-5*-sulfonate, respectively. Formation of an intramolecular hydrogen bond O3···H3 and the electron-withdrawing ability of the 7-O-sulfate group altogether allow the formation of the most stable O3-radical product for morin-7-O-sulfate. For most compounds tested, the HAT reaction at O3-H3 is highly favorable both thermodynamically and kinetically, whereas O5-H5 shows the lowest likelihood of undergoing the HAT reaction due to the lowest stability of the O5-radical product.

Concerning the kinetics, O4*-H4* in morin-5*-sulfonate shows the highest kinetic reactivity due to the activating effect of a hydrogen bond between the H atom in ·OH and the O atom in the C5*-sulfonate group. On the other hand, the slowest H-atom abstraction is predicted to occur at O2*-H2* in morin-5*-sulfonate because of the hindering effect of electrostatic repulsion between the O atom in ·OH and O3 located near the site of reaction. In most compounds excluding morin-5*-sulfonate, O3-H3 is highly reactive to the attack of ·OH. The presence of hydrogen bonding O3···H2* has a great impact on the charge stability of the TS geometry formed upon the HAT reaction at O3-H3. Since all HAT reactions initiated by the attack of ·OH are considered rapid, the scavenging activity of each compound would technically depend on its thermodynamic potential to undergo the HAT reaction. In this case, morin and morin-7-O-sulfate could be the potential candidates for use as scavengers of ·OH. Experimental evidences on the ability of morin-7-O-sulfate to scavenge ·OH are still needed. Morin may have an advantage in the higher number of the reactive OH groups, but the superior solubility in water of morin-7-O-sulfate is more preferable in biological and pharmaceutical applications.

Acknowledgements We would like to thank Dr. Akapong Suwattanamala at Burapha University for his valuable advices.

Compliance with ethical standards

Conflict of interest This statement is to declare that there are no known conflicts of interest associated with the manuscript entitled "*Exploring the transfer of hydrogen atom from kaempferol-based compounds to hydroxyl radical at ground state using PCM/DFT approach*" by Khajadpai Thipyapong and Nuttawisit Yasarawan. There has been no significant financial support for this work that could have influenced its outcome. We further confirm that there are no ethical issues to declare in this work.

References

1. Chen AY, Chen YC (2013). Food Chem 138:2099–2107
2. Alkhamees A (2013) O. Br J Pharmacol Toxicol 4:10–17
3. Shahabadi N, Mohammadpour M (2012). Spectrochim Acta A Mol Biomol Spectrosc 86:191–195
4. Pieniążek E, Kalembkiewicz J, Dranka M, Woźnicka E (2014). J Inorg Biochem 141:180–187
5. Chen Y, Zheng R, Jia Z, Ju Y (1990). Free Radic Biol Med 9:19–21
6. Amić D, Davidović-Amić D, Beslo D, Trinajstić N (2003). Croat Chem Acta 76:55–61
7. Treml J, Šmejkal K (2016). Compr Rev Food Sci Food Saf 15:720–738
8. Husain SR, Cillard J, Cillard P (1987). Phytochemistry 26:2489–2491
9. Chen J-W, Zhu Z-Q, Hu T-X, Zhu D-Y (2002). Acta Pharmacol Sin 23:667–672
10. Chen X, Deng Z, Zhang C, Zheng S, Pan Y, Wang H, Li H (2018). Food Res Int. https://doi.org/10.1016/j.foodres.2018.11.018
11. Dar RA, Naikoo GA, Hassan IU, Shaikh AMH (2016). Anal Chem Res 7:1–8
12. Li H-W, Zou T-B, Jia Q, Xia E-Q, Cao W-J, Liu W, He T-P, Wang Q (2016). Biomed Pharmacother 84:909–916
13. Doroshenko AO, Posokhov EA, Verezubova AA, Ptyagina LM (2000). J Phys Org Chem 13:253–265
14. Georgieva I, Trendafilova N, Aquino AJA, Lischka H (2006). J Phys Chem A 111:127–135
15. Marković Z, Milenković D, Đorović J, Dimitrić Marković JM, Stepanić V, Lučić B, Amić D (2012). Food Chem 135: 2070–2077
16. Yasarawan N, Thipyapong K, Ruangpornvisuti V (2014). J Mol Graph Model 51:13–26
17. Fiorucci S, Golebiowski J, Cabrol-Bass D, Antonczak S (2004). Chem Phys Chem 5:1726–1733
18. Sadasivam K, Kumaresan R (2011). Mol Phys 109:839–852
19. Frisch MJ, Trucks GW, Schlegel HB, Scuseria GE, Robb MA, Cheeseman JR, Scalmani G, Barone V, Petersson GA, Nakatsuji H, Li X, Caricato M, Marenich AV, Bloino J, Janesko BG, Gomperts R, Mennucci B, Hratchian HP, Ortiz JV, Izmaylov AF, Sonnenberg JL, Williams DF, Lipparini F, Egidi F, Goings J, Peng B, Petrone A, Henderson T, Ranasinghe D, Zakrzewski VG, Gao J, Rega N, Zheng G, Liang W, Hada M, Ehara M, Toyota K, Fukuda R, Hasegawa J, Ishida M, Nakajima T, Honda Y, Kitao O, Nakai H, Vreven T, Throssell K, Montgomery Jr JA, Peralta JE, Ogliaro F, Bearpark MJ, Heyd JJ, Brothers EN, Kudin KN, Staroverov VN, Keith TA, Kobayashi R, Normand J, Raghavachari K, Rendell AP, Burant JC, Iyengar SS, Tomasi J, Cossi M, Millam JM, Klene M, Adamo C, Cammi R, Ochterski JW, Martin RL, Morokuma K, Farkas O, Foresman JB, Fox DJ (2016) Gaussian 16 (Revision B.01). Gaussian Inc., Wallingford
20. Yanai T, Tew DP, Handy NC (2004). Chem Phys Lett 393:51–57
21. Jacquemin D, Perpète EA, Scuseria GE, Ciofini I, Adamo C (2008). J Chem Theory Comput 4:123–135
22. Shchavlev AE, Pankratov AN, Shalabay AV (2005). J Phys Chem A 109:4137–4148
23. Hao C, Tureček F (2009). J Am Soc Mass Spectrom 20:639–651
24. Li M, Xie L-F, Ju X-H, Zhao F-Q (2013). Petrol Chem+ 53:431–437
25. Yasarawan N, Thipyapong K, Ruangpornvisuti V (2016). J Mol Struct 1107:278–290
26. Marenich AV, Cramer CJ, Truhlar DG (2009). J Phys Chem B 113: 6378–6396
27. Glendening ED, Reed AE, Carpenter JE, Weinhold F (1998) NBO Version 3.1. TCI, University of Wisconsin, Madison
28. Zhao J, Zhang R (2008) In: Sabin J, Brandas E (eds) Advances in Quantum Chemistry: Applications of Theoretical Methods to Atmospheric Science, vol 55. Academic Press, San Diego, pp 177–214
29. Suwattanamala A, Ruangpornvisuti V (2009). Struct Chem 20: 619–631
30. Seyoum A, Asres K, El-Fiky FK (2006). Phytochemistry 67:2058–2070
31. Matei I, Tablet C, Ionescu S, Hillebrand M (2014). Rev Roum Chim 59:401–405
32. Anouar EH, Marakchi K, Komiha N, Kabbaj OK, Dhaouadi Z, Lahmar S (2009). Phys Chem News 45:107–113
33. Atohoun YGS, Doco RC, Houngue MTAK, Kuevi AU, Kpotin GA, Mensah J-B (2016). Am J Sci Ind Res 7:145–152
34. Dimitrić Marković JM, Milenković D, Amić D, Popović-Bijelić A, Mojović M, Pašti IA, Marković ZS (2014). Struct Chem 25:1795–1804
35. van Acker SABE, de Groot MJ, van den Berg D-J, Tromp MNJL, Donne-Op den Kelder G, van der Vijgh WJF, Bast A (1996). Chem Res Toxicol 9:1305–1312
36. Rong YZ, Wang ZW, Zhao B (2013). Food Biophys 8:90–94
37. Bondi A (1964). J Phys Chem 68:441–452

38. Parthasarathi P, Subramanian V (2006) Characterization of Hydrogen Bonding: From van der Waals Interactions to Covalency. In: Grabowski SJ (ed) Hydrogen Bonding - New Insights, vol 3. Challenges and Advances in Computational Chemistry and Physics, vol 3. Springer, Dordrecht, pp 1–50
39. Cao S, Jiang X, Chen J (2010). J Inorg Biochem 104:146–152
40. Souza RFV, De Giovani WF (2005). Spectrochim Acta A Mol Biomol Spectrosc 61:1985–1990